IEEE Access
Multidisciplinary | Rapid Review | Open Access Journal

SPECIAL SECTION ON MILLIMETER-WAVE AND TERAHERTZ PROPAGATION, CHANNEL MODELING AND APPLICATIONS

Received February 8, 2019, accepted February 25, 2019, date of publication March 7, 2019, date of current version March 26, 2019.

Digital Object Identifier 10.1109/ACCESS.2019.2903493

Mutual Coupling Reduction for Ultra-Dense Multi-Band Plasmonic Nano-Antenna Arrays Using Graphene-Based Frequency Selective Surface

BIN ZHANG[1,2,3], JOSEP M. JORNET[4], (Member, IEEE), IAN F. AKYILDIZ[3], (Fellow, IEEE), AND ZHI P. WU[1,2]

[1]School of Information Engineering, Wuhan University of Technology, Wuhan 430070, China
[2]Hubei Engineering Research Center of RF-Microwave Technology and Application, Wuhan University of Technology, Wuhan 430070, China
[3]School of Electrical and Computer Engineering, Georgia Institute of Technology, Atlanta, GA 30332, USA
[4]Department of Electrical Engineering, University at Buffalo, The New York State University, Buffalo, NY 14260, USA

Corresponding authors: Ian F. Akyildiz (ian@ece.gatech.edu) and Zhi P. Wu (z.p.wu@whut.edu.cn)

This work was supported by China Scholarship Council (CSC) under Grant 201606950051.

ABSTRACT Terahertz (THz) band provides huge bandwidth but the molecular absorptions in these frequencies cause high path losses in long-distance communications. Recently, multi-band ultra-massive MIMO (UM-MIMO) systems based on graphene-based plasmonic nano-antennas have been proposed to overcome the distance problem. In the UM MIMO systems, the mutual coupling effect is a challenging problem because of the ultra-dense integration of the multi-band nano-antenna arrays. In this paper, a graphene-based frequency selective surface (FSS) is proposed to reduce the coupling effects in dense plasmonic nano-antenna arrays for multi-band UM MIMO systems. The performance of the proposed structure is evaluated by full-wave simulation for different cases. The results show that the FSS structure has a wide stopband (−15 dB bandwidth, approximately 43%–50%) from 1.1 to 1.7 THz. By inserting the FSS structure between nano-antennas, a high isolation coefficient of −25 dB with a 15 dB fall and an envelope correlation coefficient of less than 0.01 are achieved. The field distributions and the radiation patterns are also presented to confirm that the proposed FSS structure improves the performance of the array with negligible influence on the antenna itself. Moreover, the receiving mode simulation of the array is performed with the FSS structure. It is also asymptotically shown that the mutual coupling experienced by the nano-antenna with the FSS structure is negligible even in the presence of a very large number of closely integrated elements. Finally, the technological issues are discussed for practical implementations.

INDEX TERMS Graphene, decoupling, FSS, multi-band, UM MIMO, terahertz communications.

I. INTRODUCTION

Terahertz band (0.1-10 THz) has been envisioned as one of the promising spectrum regions to enable Terabits-per-second (Tbps) links due to the increasing demand for faster data rates in future generation communication systems [1]. The available transmission bandwidth in the THz band drastically changes with the distance and the medium molecular composition [2]. For short distances, the THz-band behaves as a single transmission window with almost 10 THz bandwidth, whilst for long distances, molecular absorption delimits several transmission windows, tens to hundreds of GHz each. However, the use of THz band for communication comes with a cost of high propagation loss in free space, which combined with the low output power of THz sources, limits the communication distance. To overcome this limitation, the utilization of very dense nano-antenna arrays in Ultra-massive MIMO communication systems has been proposed recently [3]. UM MIMO systems can operate in several different ways, from ultra-narrow beamforming to ultra-massive spatial multiplexing. More interestingly, to maximize the utilization of the THz band, the concept of

The associate editor coordinating the review of this manuscript and approving it for publication was Franco Fuschini.

multi-band UM MIMO has been introduced. This technique is enabled by leveraging the tunability of novel graphene-based plasmonic devices.

Graphene is an enabling material for the realization of UM MIMO systems because of the unprecedented electrical and optical properties [4]. Compared with metal, graphene exhibits a unique frequency-dependent complex-valued conductivity which enables the propagation of Surface Plasmon Polariton (SPP) waves at THz-band frequencies [5]. SPP waves are surface-confined electromagnetic (EM) waves that result from the global oscillations of electrons on the graphene layer. The propagation speed of SPP waves is much lower than that of free-space EM waves, and, as a result, graphene-based plasmonic devices at THz frequencies are up to two orders smaller than their metallic counterparts. Among others, this feature has led to the integration of graphene-based plasmonic antenna in very small footprints. Since the first work on graphene-based nano-antennas in 2010 [6], many aspects of graphene-based nano-antennas have been explored [7]–[10]. More details are provided in Sec. II on the state of art of the graphene-based plasmonic nano-antennas. Among them, it has been shown that the resonant frequency of the graphene-based plasmonic nano-antenna can be electrically tuned [7]. As a consequence, nano-antenna arrays able to simultaneously operate at different transmission windows can be realized.

In such very dense nano-antenna array structures, mutual coupling between elements can significantly limit the array performance and ultimately limiting the communication distance. Mutual coupling effects are generally caused by radiation in free space as well as surface wave interactions from adjacent antenna elements [11]. For planar graphene-based nano-antennas, the coupling effects are mainly from surface waves and their near-field radiation. Strong coupling effects would result in a high correlation and low isolation between elements [12]. It is important to note that the graphene material demonstrates natural advantages on reduction of mutual coupling effects because of the short SPP wavelength resulting from the slow propagation speed of SPP wave. In this way, graphene-based antennas exhibit lower mutual coupling effects than metallic antenna arrays with the same distance between elements [13].

Nevertheless, the residual contributions to the total coupling from massive numbers of neighboring antennas require the development of decoupling methods and techniques. Defective ground structure (DGS) [14], [15], electromagnetic band gap (EBG) [16]–[18], metamaterials [19], [20] and frequency selective surface [21] structures are examples of common techniques that have been proposed to achieve this goal, and which we present and compare in Sec. II. Existing work mainly relies on the use of metallic structures, which introduce high losses at THz frequencies and can be challenging to integrate with graphene structures. Therefore, it is desired to again use graphene for the decoupling structure. Moreover, the tunability of graphene can be exploited to create broadband decoupling structures. For example, in [22], a graphene cloak is used to reduce the coupling effects between two dipole antennas. While the use of graphene in decoupling structures has been suggested in the related literature [23], the benefits introduced by its tunability is neither discussed nor exploited.

In our previous work [24], the graphene-based FSS structures were employed to reduce the coupling effects for the multi-band UM MIMO arrays. In that work, we provided preliminary results related to the isolation coefficient and resulting radiation diagram for the graphene-based plasmonic nano-antenna array with and without the proposed FSS structures. More results based on different parameters and cases should be presented to enrich the discussion. Furthermore, the practical consideration on the technological issues has not been yet explored.

In this paper, we present the FSS design and analytically model and simulate the proposed structure. We then investigate the performance of ultra-massive nano-antenna systems comprehensively with the FSS decoupling structures for various cases. Our results show that the FSS structure can successfully reduce the coupling effects and lower the ECC by an order of magnitude while not changing the antenna array radiation diagram. The performance of the receiving mode of the array with the FSS decoupling structure is analyzed to prove the reciprocal characteristic of the proposed structure. It is also asymptotically shown that the mutual coupling between antenna elements in ultra-dense array is negligible with proposed FSS structure in presence. The technological aspects are presented for the forthcoming implementation in practice.

The rest of this paper is organized as follows. Related work on graphene-based plasmonic nano-antennas and the mutual coupling effects is presented and compared in Sec. II. A two-band antenna array prototype model is presented, and the mutual coupling effects of this model are studied in Sec. III. The graphene-based FSS decoupling structure is proposed and analyzed in Sec. IV. Implanting the FSS structure between the antenna arrays, the performance of the array with FSS structure is investigated and the results are discussed in Sec. V. The technological issues that should be considered for practical realization are also explored in Sec. V. Finally, conclusions are drawn in Sec. VI.

II. RELATED WORK

Graphene is a two-dimensional carbon crystal that has excellent electrical conductivity, making it very well suited for propagating extremely-high-frequency electrical signals [3]. Moreover, graphene supports the propagation of THz surface plasmon polariton waves at room temperature. Motivated by these properties, the use of graphene to create plasmonic nano-antennas that can efficiently operate in the THz band is introduced. In 2010, graphene-based nano-antennas were proposed for the first time for EM nanoscale communications in terahertz band [6]. Then the radiation and scattering properties and, most importantly, the frequency tunability [7] of the graphene-based nano antenna were investigated.

Among others, it has been shown that graphene-based nano-antennas can be a good candidate for reconfigurable [8] and beamforming [9], [25] antenna arrays in communication systems. Moreover, due to the slow propagation speed of SPP waves, the size of individual antennas is up to two orders smaller than that of metallic antennas, which enables the integration in very dense nano-antenna arrays [26], [27]. Since the very small gap between nano-antennas, the mutual coupling effects between the elements are inevitable in THz antenna array.

Mutual coupling affects the array performance by limiting its beamforming capabilities and eventually restricting the communication distance. There are several techniques for mutual coupling reduction. Among them, DGS can be loaded on the ground plane of antennas to lower the coupling effects by stopping the surface current propagation [14], [15]. However, the use of DGS may affect the radiation pattern because of backward signal leakage. EBG [16]–[18] and metamaterial structures [19], [20] are usually used for reducing surface wave coupling between the antennas. FSS structures are also used in antenna array to improve the performance of the array [21], [28]. To some extent, EBG, FSS and metamaterial could be seen as one category for decoupling: periodic structure with band stop or band pass characteristics. There are some published works using FSS for decoupling in single band and low frequency antenna array. In [21], a metallic FSS wall is used to reduce the coupling effects of a 60 GHz MIMO antenna system. However, most of these metallic-based decoupling structures are mainly for small array (2 or 4 elements typically) working at frequencies lower than 0.1 THz.

For multi-band MIMO systems based on graphene-based nano-antennas, the traditional metallic decoupling methods are incapable to handle the high signal loss in THz band, let alone dynamically cover two or more working bands. Graphene decoupling structures are reported recently, but they do have shortcomings of not practically realizable [22] and not tunable for multi-band MIMO systems [23]. In this context, these literatures inspires the idea of utilizing graphene as basic material for multi-band FSS structures to reduce coupling effects of ultra-dense graphene-based nano-antenna arrays.

III. ANTENNA ARRAY DESIGN AND MUTUAL COUPLING EFFECTS

Before realizing the mutual coupling reduction, the coupling effects between the multi-band graphene-based nano-antennas are investigated. In our analysis, the graphene-based nano-antenna arrays with two and four elements are designed and employed as the platform for the study of the coupling effects. Note that the dual-band array with two or more antennas are considered here since the studies with single-band antennas are intensively reported [11]–[13] and are out of the scope of this paper. First, the complex conductivity model of graphene sheet and the dispersion relationship of SPP waves propagation are recalled and the design and analysis of graphene-based nano-antenna array is conducted. Then, mutual coupling effects between adjacent nano-antennas are investigated. Several parameters are presented to evaluate the impact of coupling effects.

A. GRAPHENE-BASED PLASMONIC NANO-ANTENNA DESIGN

The proposed multi-band nano-antenna array consists of several sub-sets of nano-antennas working at different frequency bands. There are different types of the sub-array schemes, which require the antenna elements to be capable to switch from one working band to other bands. Thus, the basic element of the sub-array should be frequency-reconfigurable. This is achieved by leveraging the frequency tunability of graphene.

The surface conductivity of graphene is described by using the Kubo formula and is a function of frequency $f = \omega/2\pi$, Fermi energy E_f and relaxation time τ. The total conductivity is given by [5]

$$\sigma^g = \sigma^g_{intra} + \sigma^g_{inter}, \tag{1}$$

$$\sigma^g_{intra} = \frac{2e^2 k_B T}{\pi\hbar^2} \ln\left(2\cosh\left(\frac{E_F}{2k_B T}\right)\right) \frac{i}{\omega + i\tau_g^{-1}}, \tag{2}$$

$$\sigma^g_{inter} = \frac{e^2}{4\hbar}\left(H\left(\frac{\omega}{2}\right) + i\frac{4\omega}{\pi}\int_0^\infty \frac{H(\Xi) - H\left(\omega/2\right)}{\omega^2 - 4\Xi^2} d\Xi\right), \tag{3}$$

and

$$H(a) = \frac{\sinh\left(\hbar a/k_B T\right)}{\cosh\left(E_F/k_B T\right) + \cosh\left(\hbar a/k_B T\right)}, \tag{4}$$

where $\hbar = h/2\pi$ is the normalized Planck's constant, e is the electron charge, k_B is the Boltzmann constant, T stands for temperature. The conductivity can easily be tuned by applying a bias voltage or chemical doping. The propagation of TM SPP waves follows the simplified dispersion relationship below [29]

$$-i\frac{\sigma_g}{\omega\varepsilon_0} = \frac{\varepsilon_1 + \varepsilon_2}{k_{spp}}, \tag{5}$$

where ε_1 and ε_2 denote the permittivity values of two media above and below the graphene sheet, and k_{spp} is the complex propagation constant of TM SPP waves. The SPP wavelength is calculated by $\lambda_{spp} = 2\pi/\mathrm{Re}\left[k_{spp}\right]$. By changing the Fermi energy, the conductivity is dynamically tuned, then the antenna based on graphene becomes frequency reconfigurable.

In Fig. 1a, we illustrate the reference antenna design that we utilize in this paper. For convenience, a dipole patch antenna is chosen as the basic antenna element. The dipole patches made with single layer graphene are paved on a SiO_2 substrate with thickness of 5 μm. The graphene-based patch is defined by length $L_{ant} = 11$ μm and width $W_{ant} = 5$ μm. The gap between the two arms is 1 μm. The frequency response of the antenna is reconfigurable with respect to

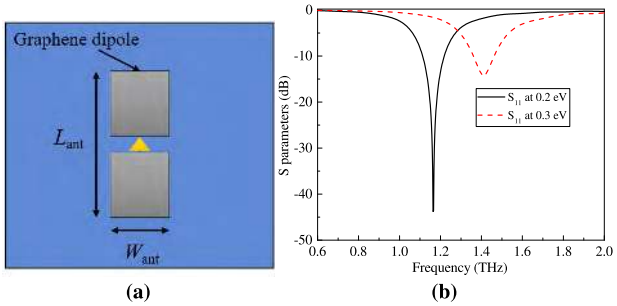

FIGURE 1. Graphene-based plasmonic nano-antenna. (a) Scheme of the antenna and (b) the return loss of antenna being tuned with different chemical potential levels.

biasing or chemical doping. The simulation of the antenna is conducted by using a full-wave analysis software package CST. Fig. 1b gives the reflection coefficients S_{11} of the antenna while the chemical potential is set as 0.2 eV and 0.3 eV, respectively. One can observe that the graphene-based plasmonic nano-antenna with fixed physical dimensions demonstrates multi-band property while the antenna is tuned at different Fermi energy levels.

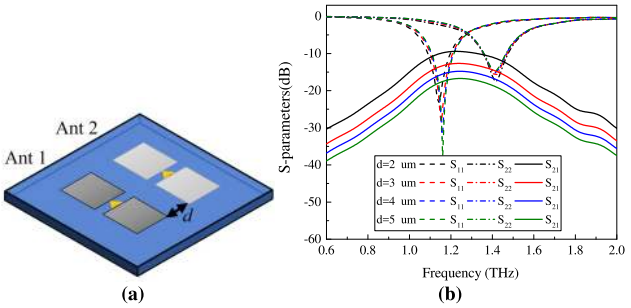

FIGURE 2. The two-element two-band graphene-based plasmonic nano-antenna array. (a) Schematic diagram of the array with separation distance *d*. (b) *S*-parameter responses of the antenna array model.

B. MUTUAL COUPLING BETWEEN ADJACENT NANO-ANTENNAS

In multi-band UM MIMO system, there may be thousands of antenna elements, but the dominant mutual coupling effects usually exist between the two adjacent elements in most cases. Here, we consider two different cases: dual-band two-element and dual-band four-element linear arrays. In the first case, two antennas with the same dimension but being tuned with different energy levels are placed within a certain distance, as shown in Fig. 2a. For the array with four elements, the two antennas are linearly interleaved with a uniform space between them, as shown in Fig. 3a. The N-antenna array is seen as a N-port system. We can use the transmission coefficient between two ports to describe the mutual coupling effects of the system. There are several parameters to describe the mutual coupling effects for the two-element array. Among them, the scattering parameter S_{21}, also called as the isolation coefficient, is a basic form to evaluate the effects. The S_{21} responses with various distances between antenna elements are analyzed for both cases.

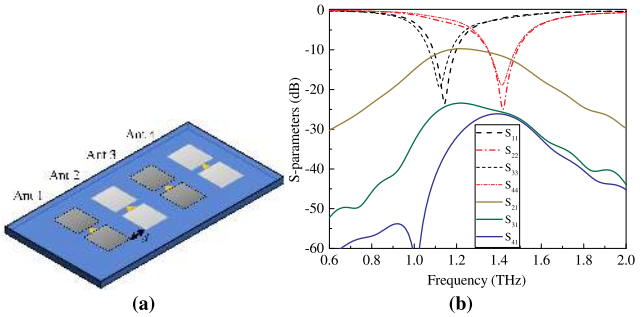

FIGURE 3. The two-element two-band graphene-based antenna array. (a) Schematic diagram of the array with separation distance of *d*. (b) S-parameter responses of the antenna array model with separation distance of 2 μm.

For the two-element case, the S_{21} responses are obtained between two elements separated by an edge-to-edge distance ranging from 2 to 4 μm. The results show that at distance of 2 μm, approximately one fifth of the SPP wavelength, the peak value of S_{21} curve is -9.4 dB, which is not acceptable for an array system. As the distance rises, the isolation between the two elements decreases to -17 dB, as shown in Fig. 2b. For the array with four antennas, we choose antenna 1 as the object of study and present S_{21}, S_{31}, S_{41} to show the influence from other elements. In Fig. 3b, we can see that S_{31} and S_{41} give a low peak of -25 dB, which is negligible compared with S_{21}. We only need to tackle the problem of isolation between the two adjacent elements. These S_{21} values are insufficient due to the low efficiency and sophistication for THz multi-band UM MIMO system. Thus, there would have potential to reduce the mutual coupling by using decoupling structure like FSS but not increasing space between antenna elements at the same time.

The envelope correlation coefficient [12], calculated from the simulated scattering parameters, is a measure for evaluating the coupling effects from each other element when operated simultaneously. For the two-band two-element array model, the envelope correlation coefficient ρ is calculated from formula [30]:

$$\rho = \frac{|S_{11}{}^{*}S_{12} + S_{21}{}^{*}S_{22}|}{\left(1 - |S_{11}|^2 - |S_{21}|^2\right)\left(1 - |S_{22}|^2 - |S_{12}|^2\right)}. \quad (6)$$

For the four-element case, the ECC is obtained between any two elements.

The antenna radiation pattern, i.e., the power radiated by antenna as a function of space coordinates, is another significant feature that is affected by mutual coupling effects. Especially in antenna arrays, the far-field radiation pattern is strongly based on the pattern of a single element. In the following sections, the radiation pattern is also presented to evaluate the decoupling effects.

IV. GRAPHENE-BASED FSS DESIGN

In this section, we present the design of the graphene-based frequency selective surface structure to reduce the

mutual coupling effects. FSS structure is known as its band stop or band pass characteristics depending on the periodic patch or slot with certain patterns. To some extent, a FSS behaves as a spatial filter. For band-stop purpose, patch-based FSSs are employed in this case. A unit cell is the most basic structure of FSS. The performance of a full-dimension FSS structure is achieved by extending the unit cell result with Floquet's principle [31]. Commonly, the resonance wavelength of FSS, λ_c, is calculated approximately as twice the element length by $L_{FSS} \simeq \lambda_c/2$ [31]. However, in a practical way, the element length is not exactly half wavelength due to the substrate effect and dispersive nature of SPP waves on graphene. The working frequency of the FSS is determined by the element length, substrate permittivity and substrate dimensions. Among them, the patch length is the significant one that can directly influence the working frequency of the FSS structure. Also, the width of element is usually much smaller than the length.

Here, we propose a graphene-based cross patch FSS structure working at THz frequencies. For multi-band and reconfigurable purpose, graphene becomes a reasonable choice to be employed as patch materials in FSS structure. We can achieve multi-band with one fixed-size FSS patch/slot by simply modifying the chemical potential level. In this case, a cross patch is selected as the unit cell element for its cross-polarization character, with arm length $L_{cross} = 10.97\ \mu$m and width $W_{cross} = 3\ \mu$m. The length of the square substrate is $a = 11\ \mu$m. In Fig. 4a, the schematic of the proposed FSS structure is presented. For better resonance and wider working band, four layers of graphene-based cross patches are used in the design of the FSS. Two graphene cross patches with same energy level and one SiO_2 film (thickness is 0.2 μm) between the patches compose a FSS sandwich structure. There are two sandwich structures attached on each side of a 0.6-μm-thick polysilicon substrate with permittivity of 11.9. For multi-band UM MIMO system, the Fermi energy level should be chosen carefully to make the FSS patch resonate at the working bands of the aforementioned antenna array. Here, we set 0.2 eV and 0.3 eV as graphene chemical potential for each sandwich structure. Temperature of graphene is set as 300 K and the relaxation time is 0.5 ps. It should be noted that due to the coupling effects between the FSS patches the working band of the structure is not simply the combination of two resonant frequencies of FSS at 0.2 eV and 0.3 eV. Also, as the distance between the patches is very small, the two patches in the same sandwich structure are strongly coupled as a capacitor, which results in a frequency shift of the FSS structure.

The full wave simulation of the FSS structures is carried out by CST Microwave Studio. A planar wave is used as input signal to get the frequency response of the structure. Noted that only normal incidence is considered in the simulation. The simulated performances of the FSS are given in Fig. 4. It is observed that the proposed FSS decoupling structure has a wide −15 dB bandwidth from 1.1 THz to 1.7 THz. The −10 dB bandwidth is more than 1 THz

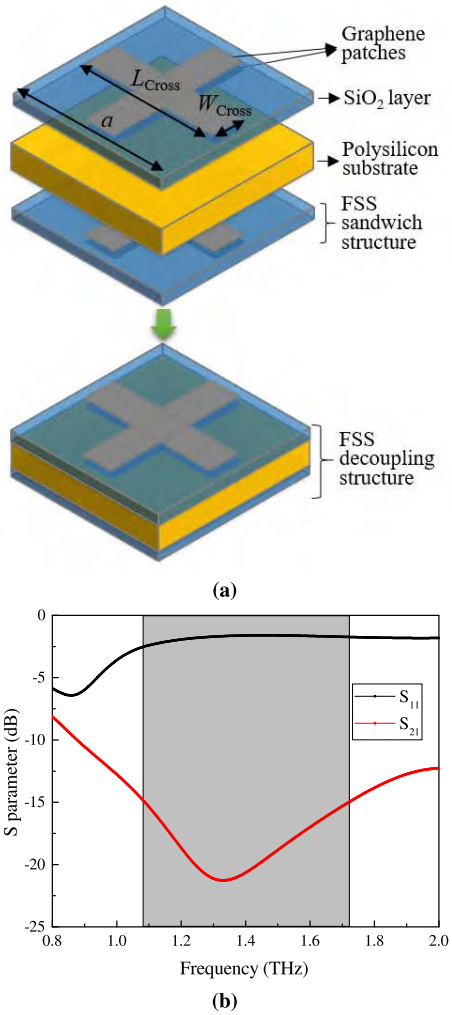

FIGURE 4. The proposed FSS decoupling structure for multi-band array: (a) configuration diagram and (b) simulated S-parameters results. Grey area is the −15 dB bandwidth.

starting from 0.9 THz, which efficiently covers both target frequency ranges: 1.1 THz-1.25 THz and 1.35 THz-1.5 THz. Furthermore, we can utilize this FSS structure to cover other frequency ranges by properly modifying the energy levels of graphene patches. The proposed FSS structure shows the potential to be employed for reduction of coupling effects of the proposed antenna array or even any other antenna arrays with different working bands.

V. PERFORMANCE ANALYSIS AND DISCUSSION

The decoupling performance of the proposed FSS structure is presented by mounting it between the two adjacent antenna elements of the multi-band UM MIMO systems in this section. The obtained isolation magnitude is approximately −10 dB with separation distance of 2 μm presented in previous sections, which is not acceptable and can certainly be improved. What is more, due to the high substrate permittivity, the SPP wave energy is mostly guided backward and part of the energy is stored and transmitted in the substrate. In this

context, we propose to insert the FSS decoupling structure into the substrate of the nano-antenna array to block the wave propagation between the elements. Moreover, it is practically feasible to insert a FSS structure into a dielectric substrate. Here, we consider both two-element and four-element arrays to study the decoupling performance of FSS structures. The edge-to-edge distance between the two adjacent elements is set as 2 μm, which is approximately one fifth of the SPP wavelength. Then, the receiving mode performance of the two-element array is investigated with the FSS structure in place. Finally, the asymptotic behavior in massive multi-band arrays is evaluated in this section.

A. MULTI-BAND GRAPHENE-BASED ARRAY WITH TWO ELEMENTS

The two-element two-band antenna array with FSS decoupling structure is simulated in CST microwave studio. The minimum mesh cell of the simulation model is defined as 0.15 μm for accuracy, which is far smaller than the SPP wavelength. Besides the standard S-parameters, electric and magnetic field monitors are set to obtain electric-field and surface current distribution. Also, an open boundary condition is employed to study the far-field distribution.

In Fig. 5b, the S-parameters are illustrated for four scenarios: nano-antenna array without FSS structure, antenna array with FSS structure mounted between elements and antenna array with FSS structure inserted into substrate with insert depth of 2 and 4 μm. It is clearly seen that there is a maximum 5 dB drop of isolation coefficient after using the proposed FSS structure. With insert depth rises from 0 to 4 μm, the max isolation decreases from the original -9.4 dB to approximately -25 dB, which is more than a 15 dB drop. It should be noted that using FSS structures in nano-antenna array systems lead to a resonant frequency shift of 6.9% and 8.5% for Antenna 1 and Antenna 2, respectively, compared to the original nano-antenna resonant frequencies, as shown in Fig. 5b. This is a result from the coupling between the antenna element and FSS structure. What is more, the max value of ECC declines from 0.25 to less than 0.03 at the frequency range of interest, as shown in Fig. 5c.

Mutual coupling effects can directly lead to the change of electric and magnetic field distribution. In Fig. 6a-6h, electric field distributions of the array with and without FSS are presented as well as the surface current density plot. One can observe that there is strong induced current and field distribution on antenna 2 when antenna 1 is excited, and vice versa. More importantly, part of electric field is absorbed and guided through the high permittivity substrate. After inserting the FSS between the elements, the induced fields are efficiently blocked and the surface current density on terminated antenna is also been suppressed by the FSS decoupling structure, as shown in Fig. 6.

The radiation patterns are also strongly affected due to the coupling between antenna elements. Fig. 7 shows the radiation patterns of Antenna 1 and 2 at the targeted working frequencies. Three cases are considered to validate the

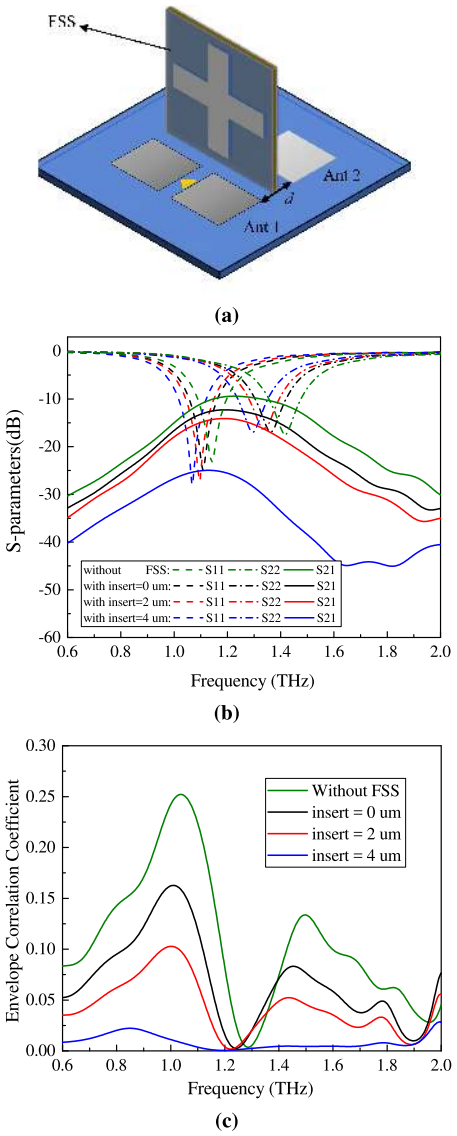

FIGURE 5. The two-element antenna array with mounted FSS decoupling structures. (a) Configuration scheme of the array. (b) S-parameters and (c) ECC curves of the array without FSS and with FSS insert depth of 0 μm, 2 μm and 4 μm.

reduction of mutual coupling effects because of the FSS decoupling structure: an isolated antenna, an antenna in array without FSS and an antenna in array with FSS. Particularly, both the E-plane and H-plane patterns are given. In Fig. 7a and Fig. 7c, the E-planes of both antennas are slightly influenced due to the arrangement of the array elements. However, the coupling between the elements would strongly affect the H-plane of the radiation pattern, as shown in Fig. 7b and Fig. 7d. After inserting of the FSS structure, both radiation patterns are recovered well as if the antennas are originally isolated without coupling. The max variation of the gain values of both antennas is lower than 0.1 dB. The results reveal that the coupling effects have negligible influence on E-plane radiation pattern of antenna and FSS structure can efficiently recover the H-plane pattern.

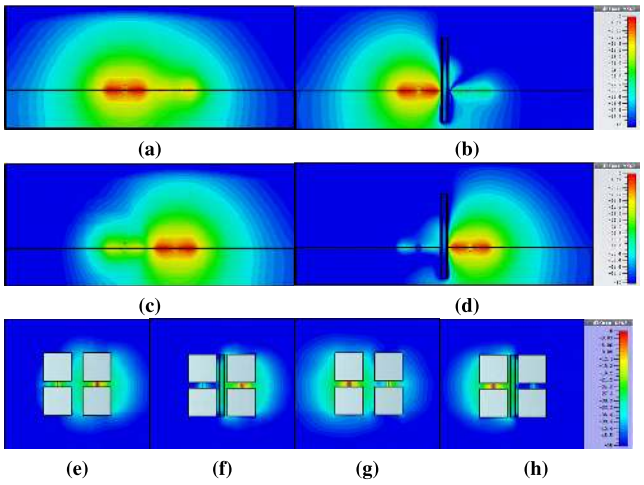

FIGURE 6. Electric field distribution of the two-element array cross section: (a) Antenna 1 working at 1.16 THz without FSS in place and (b) with FSS inserted by 4 μm. (c) Antenna 2 working at 1.41 THz without FSS in place and (d) with FSS inserted by 4 μm. Surface current distribution of the two-element array: (e) Antenna 1 working at 1.16 THz without FSS in place and (f) with FSS inserted by 4 μm. (g) Antenna 2 working at 1.41 THz without FSS in place and (h) with FSS inserted by 4 μm.

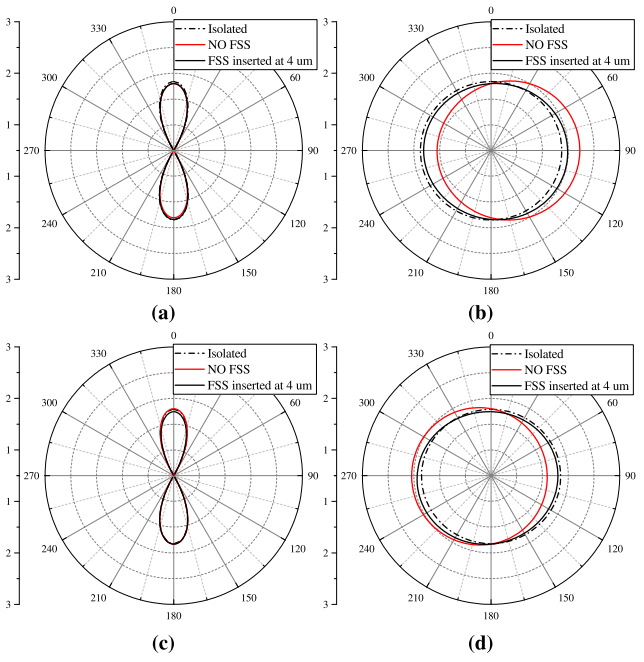

FIGURE 7. Simulated radiation patterns of the two-element array: (a) E-plane and (b) H-plane of Antenna 1 working at 1.16 THz. (c) E-plane and (d) H-plane of Antenna 2 working at 1.41 THz.

B. MULTI-BAND GRAPHENE-BASED ARRAY WITH FOUR ELEMENTS

For the case with four nano-antennas, three FSSs are employed for the reduction of coupling effects among the elements. Fig. 8a shows the configuration of the four-element array with the FSS decoupling structures in place. Here, only isolation S_{21} between Antenna 1 and 2 is considered in this subsection. The same simulation settings as in the previous

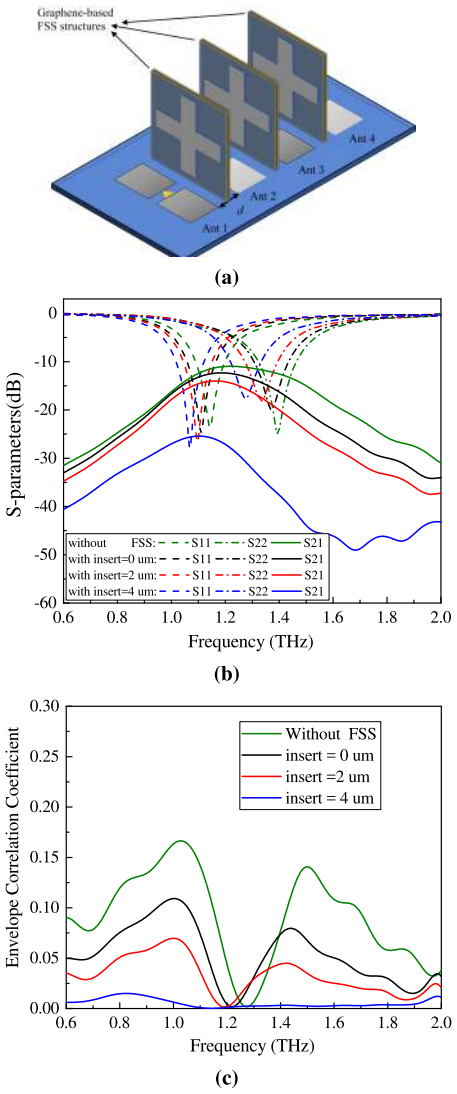

FIGURE 8. The four-element antenna array with mounted FSS structures. (a) Configuration of the array. (b) S-parameters and (c) ECC curves of the array without FSS and with FSS insert depth of 0 μm, 2 μm and 4 μm.

case are employed for precise results. In Fig. 8b, the isolation coefficients show a drop of 15 dB after using FSS decoupling structure. However, as there are two FSS structures being mounted at both sides of Antenna 2, the return loss S_{22} displays a max frequency shift of 8.9% which is slightly greater than the one in the two-element scenario. Moreover, the ECC plot is given in Fig. 8c with a max value of less than 0.2 without the FSS placed in the array, while the value decreases to approximately 0.02 with the FSS inserted into the array substrate.

In Fig. 9, the electric and surface current distribution are presented for the four-element case. Antenna 1 and 2 are selected as the study subjects. As shown in Fig. 9a-9d, the presence of the FSS structures well suppresses the coupled fields from the excited antenna to the terminated one. It is worth noting that Antenna 2 is surrounded by two FSS structures, which can reduce the coupling effects from

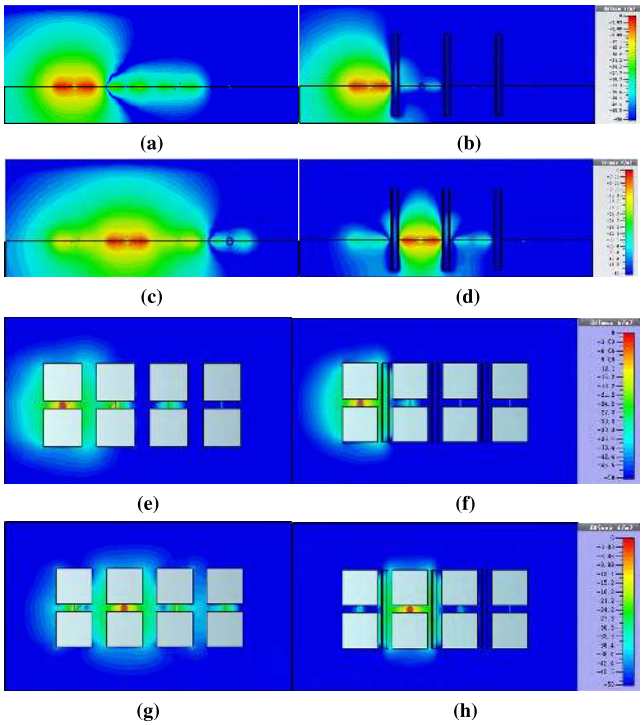

FIGURE 9. Electric field distribution of the four-element array: (a) Antenna 1 working at 1.16 THz without FSS in place and (b) with FSS in place; (c) Antenna 2 working at 1.41 THz without FSS in place and (d) with FSS in place. Current distribution of the four-element array: (e) Antenna 1 working at 1.16 THz without FSS in place and (f) with FSS in place; (g) Antenna 2 working at 1.41 THz without FSS in place and (h) with FSS in place.

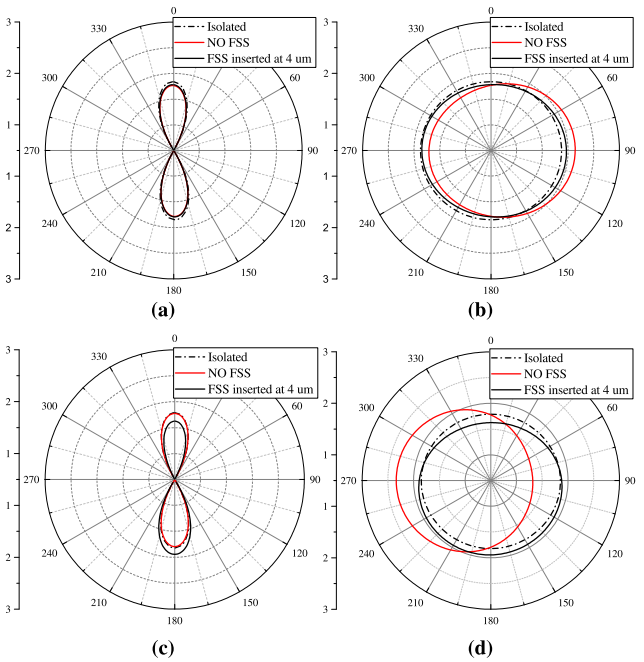

FIGURE 10. Radiation patterns of four-element array: (a) E-plane and (b) H-plane of antenna 1 working at 1.14 THz. (c) E-plane and (d) H-plane of antenna 2 working at 1.4 THz.

adjacent elements simultaneously. Reduction of mutual coupling effects is achieved as shown in Fig. 9e-9h. The induced surface current is efficiently blocked by the FSS structures, as shown in Fig. 9e-9h.

The radiation patterns of Antenna 1 and 2 in the four-element array are illustrated in Fig. 10. For isolated antennas, typical patterns of dipole antenna are given, both E-plane and H-plane. The mutual coupling effects brought by adjacent elements show huge impact on the radiation patterns of antennas. By using the FSS structures, the radiation patterns are well restored by placing the FSS structures in the array, as shown in Fig. 10a-10d. The max variation of antenna gain values brought by the FSS structure is approximately 0.2 dB in this case. Since Antenna 2 is placed between two FSS structures, part of the energy are blocked by the FSSs. Moreover, the E-plane radiation pattern of Antenna 2 with FSS in place is slightly guided to the substrate of antenna array, as plotted in Fig. 10c, due to the substrate is acting as a dielectric lens in this structure.

C. ANTENNA PERFORMANCE IN RECEIVING MODE

To validate the performance of the FSS structure in a receive antenna array system, we also perform the simulation to obtain the induced current signals at the antenna excitation port. Here we take the two-element array as the platform for loading the FSS decoupling structure in this case. Based on the radiation results obtained before, a far field source is defined as the background electromagnetic wave. The distance between the far field source and the receiving 2-element antenna array is set as 80 μm, which is far enough to make the source located in the Fraunhofer zone. Then the wave front of the far field source is approximately considered as a plane wave. As a result, the induced current signals are observed at the receiving antenna ports when the receiving array is illuminated by the defined far field source above.

As seen in Fig. 11a, the current signal responses of both antenna elements are obtained from the simulation. We demonstrate the original current signal plot at the transmitting end in the Fig. 11b. It is seen that the Antenna 1 displays a current signal with peak at 1.2 THz, which is very close to that of the original current curve at 1.18 THz. Similarly, the port current peak of Antenna 2 occurs at approximately 1.45 THz, which suggests a very small shift of 0.03 THz from the original incident wave frequency 1.42 THz. The comparison shows that when illuminated by the incident wave with the same working band, the receiving array elements with the FSS structure show the same port current peaks at the desired frequency. It should be noted that the induced current magnitude is not in the same order of the excitation signals due to the propagation loss and the relatively low radiation efficiency (approximately 2%) of the graphene plasmonic nano-antenna.

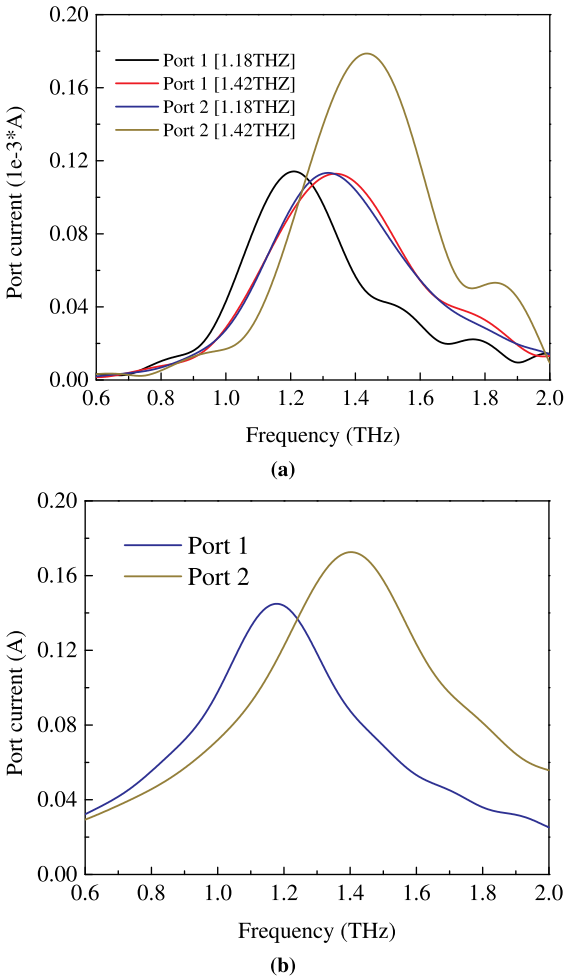

FIGURE 11. The simulated port current signals of the 2-element array system at the receiving and transmitting mode. (a) The current signals of port 1 and 2 when the array is illuminated with background EM waves resonating with working frequencies of 1.18 THz and 1.42 THz, respectively. (b) The original port current signals of both antenna elements as transmitters.

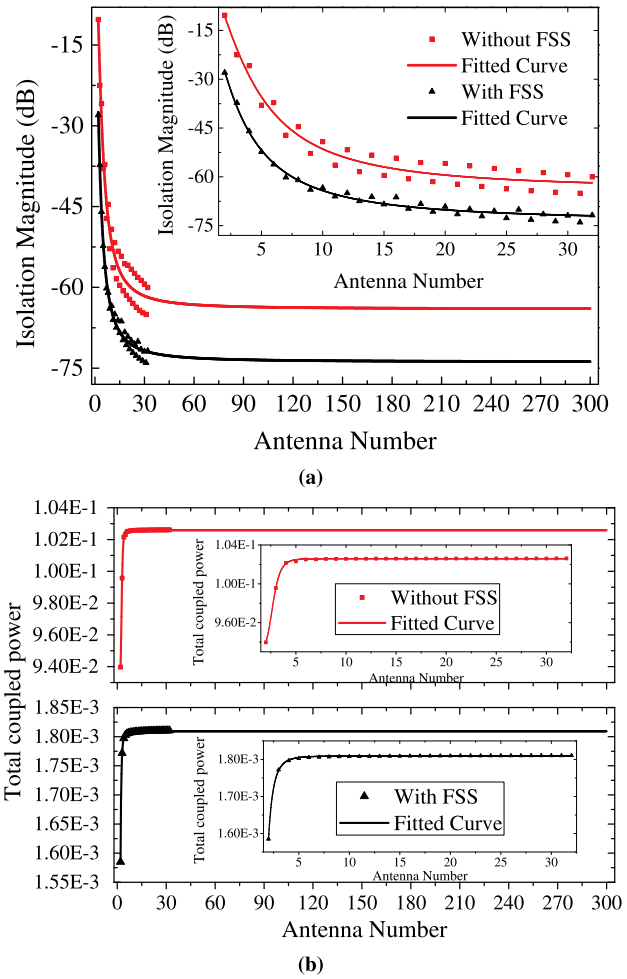

FIGURE 12. Asymptotic results over different antenna numbers. (a) Magnitude of isolation coefficient data and fitted curves. (b) Total coupled power results and fitted curve over antenna number.

D. ASYMPTOTIC BEHAVIOR IN MASSIVE MULTI-BAND ARRAYS

To evaluate the performance of the proposed FSS structures when the antenna number increases to infinity, isolation coefficients of a linear array with 32 elements are simulated and analyzed. Then the asymptotic behavior of the ultra-massive multi-band array is foretold by a using curve fitting technique.

In this case, the two antennas with different working bands are interleaved along one direction and the FSS structures are placed in between the antennas. Fig. 12a plots the magnitudes of isolation coefficients between Antenna 1 and Antenna N. Two cases are considered in this plot, the array with and without decoupling structures. In general, the magnitude of the isolation coefficient will be smaller with the antenna number increasing, which is suitable to be described with a curve regression technique. Among the available fitting techniques in the software package Origin, the Logistic regression provides the best fitting for the isolation magnitudes. We can observe that the isolation coefficients between the elements plunge with the increasing of antenna number from 2 to 32. Then the curve decreases with lower bound of -64 dB when antenna number increases from 2 to 300. It is predictable the magnitudes of the isolation data would fall gently and verge to a constant according the fitted curves. It is worth noting that there is regularly fluctuation of the magnitude values, which is resulted from the interleave arrangement of the array. With the FSS structures mounted in array, the trend declines drastically and ends up with a lower bound of -74 dB, which is smaller than the curve in the case that without the FSS. This confirms that the FSS structures work well with decoupling and the coupling effects between distant elements are insignificant.

Moreover, the total effects on Antenna 1 from other antennas are calculated and analyzed. In detail, we sum up all isolation coefficients cumulatively between Antenna 1 and Antenna N. The isolation coefficient S_{NM} denotes the power ratio from port N to M due to the reciprocity of S-parameters. Consider an array with uniform excitation power P_0 at each

antenna port, isolation between Antenna 1 and Antenna N is

$$S_{N1}(dB) = 10\log_{10}\left(|S_{N1}|^2\right) = 10\log_{10}\left(\frac{P_N}{P_0}\right), \quad (7)$$

where $S_{N1}(dB)$ is the isolation in dB and $|S_{N1}|$ is the linear value of the isolation coefficient. P_N denotes the coupled power from Antenna N to Antenna 1. Set P_0 as 1, then the total coupled power on Antenna 1 is written as

$$P_{total} = \sum_{i=2}^{N} P_i = \sum_{i=2}^{N} |S_{i1}|^2. \quad (8)$$

In this way, we obtain the total influence on Antenna 1 from all neighboring antennas when the number of array elements increases.

In Fig. 12b, the total coupled power is presented for two cases, before and after employing FSS structures in array. The enlarged views of the original data are plotted as well in insets. The results indicate the coupled power verges to a constant when the antenna number increases. The asymptotic total power percentage from neighboring antenna elements is 0.1026 and 0.00181 with and without FSS decoupling structures, respectively. It is also observed from the inset figures that the total coupled energy verges to a constant at the antenna number of 6, which validates the dominating coupling effects are mainly from neighboring and near distance elements. With the FSS decoupling structure in place, one can forecast that the total coupled power from all other elements in one array would verge to a very small constant, compared to the case without FSS, when antenna number increases to infinity. Furthermore, the graphene-based FSS structure can cover the transmission band of interest by properly tuning the Fermi energy level, which suggests the proposed FSS decoupling structure is able to handle the arrays with increasing number of working bands at the same time.

E. TECHNOLOGICAL REALIZATION

The complicated structure of the proposed graphene-based plasmonic nano-antenna array as well as the FSS may raise the concern on the technological issues for practical realization. In this subsection, we discuss the technological aspects to be considered in the practical implementation.

The high-quality graphene can be easily grown on copper substrate using the chemical vapor deposition (CVD) method [32], [33]. Then, the graphene sheet is transferred to the desired substrate, silicon dioxide in our work, with the help of the polymethyl methacrylate (PMMA). For the sandwich structure in Fig. 4a in our design, it is expected that high-quality single-layer graphene can be transferred to the both sides of the SiO_2 substrate. The minimum dimension of the whole system, including the graphene-based nano-antenna and frequency selective surface, is at the order of dozens of nanometer, which is totally achievable for the focused ion beam (FIB) technique [33], [34]. The FIB technique is able to etch the un-wanted area of graphene with a nano-meter size precision. In this way, the graphene-based plasmonic nano-antenna and the graphene-based frequency selective surface could be well defined. Once the graphene-based plasmonic nano-antenna is obtained from the CVD and FIB techniques, the excitation needs to be defined for the antenna. There are two widely reported feeding mechanisms for the graphene-based plasmonic nano-antennas, the photoconductive source and the graphene-gated high-electron-mobility-transistor (HEMT) source [35]. The photoconductive source is more suitable for the graphene-based dipole antenna in this paper.

In this paper, the parameters of graphene are selected carefully to be consistent with the practical values. The relaxation time of graphene is set as 0.5 ps [33], [36], which is consistent with the practical value from the Raman spectra analysis for a CVD graphene sheet deposited on SiO_2 substrates at room temperature (300 K) [33]. The Fermi energy levels of graphene used for the two working bands in our work are 0.2 and 0.3 eV, respectively. This is realized by applying a static electric field between graphene and an electrode at a proper position. More importantly, these values can be practically realized because they are well within the theoretical maximum Fermi energy level for a certain substrates (0.45 eV for SiO_2) [37].

VI. CONCLUSIONS

In summary, a graphene-based FSS structure has been proposed to reduce the mutual coupling effects of a multi-band UM MIMO antenna array. Multiple Fermi energy levels of graphene are carefully selected to achieve the multi-band coverage. The mutual coupling effects have been reduced by mounting the FSS structure between the array elements of the UM MIMO array. Then the isolation is further improved by inserting the FSS decoupling structure into the substrate to block the electromagnetic wave propagation in the substrate. The results have shown that both coupled electric and magnetic fields are eliminated by the FSS decoupling structure. Moreover, it has been proved that the radiation performances of the nano-antennas are insignificantly influenced with the FSS in place. The receiving mode performance of the array with the FSS decoupling structure has been analyzed to prove the reciprocal characteristic of the proposed structure. It has also asymptotically shown that the mutual coupling between antenna elements in ultra-dense array is negligible with proposed FSS structure in presence. The technological aspects have been presented for the future practical implementation. Although this structure has been designed for a dual-band UM MIMO array, we can extend the working band of the structure by adjusting the Fermi energy levels of graphene patches to other desired frequencies.

REFERENCES

[1] I. F. Akyildiz, J. M. Jornet, and C. Han, "Terahertz band: Next frontier for wireless communications," *Phys. Commun.*, vol. 12, pp. 16–32, Sep. 2014.

[2] J. M. Jornet and I. F. Akyildiz, "Channel modeling and capacity analysis for electromagnetic wireless nanonetworks in the terahertz band," *IEEE Trans. Wireless Commun.*, vol. 10, no. 10, pp. 3211–3221, Oct. 2011.

[3] I. F. Akyildiz and J. M. Jornet, "Realizing Ultra-Massive MIMO (1024 × 1024) communication in the (0.06–10) Terahertz band," *Nano Commun. Netw.*, vol. 8, pp. 46–54, Jun. 2016.
[4] A. K. Geim and K. S. Novoselov, "The rise of graphene," *Nature Mater.*, vol. 6, no. 3, pp. 183–191, 2007.
[5] G. W. Hanson, "Dyadic Green's functions and guided surface waves for a surface conductivity model of graphene," *J. Appl. Phys.*, vol. 103, no. 6, pp. 064302-1–064302-8, Mar. 2008.
[6] J. M. Jornet and I. F. Akyildiz, "Graphene-based nano-antennas for electromagnetic nanocommunications in the terahertz band," in *Proc. 4th Eur. Conf. Antennas Propag. (EuCAP)*. Barcelona, Spain, 2010, pp. 1–5.
[7] I. Llatser, C. Kremers, A. Cabellos-Aparicio, J. M. Jornet, and E. Alarcón, and D. N. Chigrin, "Graphene-based nano-patch antenna for terahertz radiation," *Photon. and Nanostruct.-Fundam. Appl.*, vol. 10, no. 4, pp. 353–358, Oct. 2012.
[8] M. Tamagnone, J. S. Gómez-Díaz, J. R. Mosig, and J. Perruisseau-Carrier, "Reconfigurable terahertz plasmonic antenna concept using a graphene stack," *Appl. Phys. Lett.*, vol. 101, no. 21, Nov. 2012, Art. no. 214102.
[9] Z. Xu, X. Dong, and J. Bornemann, "Design of a reconfigurable MIMO system for THz communications based on graphene antennas," *IEEE Trans. THz Sci. Technol.*, vol. 4, no. 5, pp. 609–617, Sep. 2014.
[10] B. Zhang, J. Zhang, C. Liu, Z. Wu, and D. He, "Equivalent resonant circuit modeling of a graphene-based bowtie antenna," *Electronics*, vol. 7, no. 11, p. 285, Oct. 2018.
[11] Z. Qamar, U. Naeem, S. A. Khan, M. Chongcheawchamnan, and M. F. Shafique, "Mutual coupling reduction for high-performance densely packed patch antenna arrays on finite substrate," *IEEE Trans. Antennas Propag.*, vol. 64, no. 5, pp. 1653–1660, May 2016.
[12] M. S. Sharawi, "Printed multi-band MIMO antenna systems and their performance metrics," *IEEE Antennas Propag. Mag.*, vol. 55, no. 5, pp. 218–232, Oct. 2013.
[13] L. Zakrajsek, E. Einarsson, N. Thawdar, M. Medley, and J. M. Jornet, "Design of graphene-based plasmonic nano-antenna arrays in the presence of mutual coupling," in *Proc. 11th Eur. Conf. Antennas Propag.*, Paris, France, 2017, pp. 1381–1385.
[14] K. Wei, J.-Y. Li, L. Wang, Z.-J. Xing, and R. Xu, "Mutual coupling reduction by novel fractal defected ground structure bandgap filter," *IEEE Trans. Antennas Propag.*, vol. 64, no. 10, pp. 4328–4335, Oct. 2016.
[15] D. Guha, C. Kumar, and S. Pal, "Improved cross-polarization characteristics of circular microstrip antenna employing arc-shaped defected ground structure (DGS)," *IEEE Antennas Wireless Propag. Lett.*, vol. 8, no. , pp. 1367–1369, 2009.
[16] F. Yang and Y. Rahmat-Samii, "Microstrip antennas integrated with electromagnetic band-gap (EBG) structures: A low mutual coupling design for array applications," *IEEE Trans. Antennas Propag.*, vol. 51, no. 10, pp. 2936–2946, Oct. 2003.
[17] H. S. Farahani, M. Veysi, M. Kamyab, and A. Tadjalli, "Mutual coupling reduction in patch antenna arrays using a UC-EBG superstrate," *IEEE Antennas Wireless Propag. Lett.*, vol. 9, pp. 57–59, 2010.
[18] M. Coulombe, S. F. Koodiani, and C. Caloz, "Compact elongated mushroom (EM)-EBG structure for enhancement of patch antenna array performances," *IEEE Trans. Antennas Propag.*, vol. 58, no. 4, pp. 1076–1086, Apr. 2010.
[19] X. M. Yang, X. G. Liu, X. Y. Zhou, and T. J. Cui, "Reduction of mutual coupling between closely packed patch antennas using waveguided metamaterials," *IEEE Antennas Wireless Propag. Lett.*, vol. 11, pp. 389–391, 2012.
[20] D. Gangwar, S. Das, and R. L. Yadava, "Reduction of mutual coupling in metamaterial based microstrip antennas: The progress in last decade," *Wireless Pers. Commun.*, vol. 77, no. 4, pp. 2747–2770, Aug. 2014.
[21] R. Karimian, A. Kesavan, M. Nedil, and T. A. Denidni, "Low-mutual-coupling 60-GHz MIMO antenna system with frequency selective surface wall," *IEEE Antennas Wireless Propag. Lett.*, vol. 16, pp. 373–376, 2017.
[22] G. Moreno, H. M. Bernety, and A. B. Yakovlev, "Reduction of mutual coupling between strip dipole antennas at terahertz frequencies with an elliptically shaped graphene monolayer," in *Proc. IEEE Int. Symp. Antennas Propag. (APSURSI)*, Jun./Jul. 2016, pp. 887–888.
[23] J. Ghosh and D. Mitra, "Mutual coupling reduction in planar antenna by graphene metasurface for THz application," *J. Electromagn. Appl.* , vol. 31, no. 18, pp. 2036–2045, Dec. 2017.
[24] B. Zhang, J. M. Jornet, I. F. Akyildiz, and Z. P. Wu, "Graphene-based frequency selective surface decoupling structure for ultra-dense multi-band plasmonic nano-antenna arrays," in *Proc. 5th ACM Int. Conf. Nanosc. Comput. Commun. (NANOCOM)*. Reykjavik, Iceland, Sep. 2018, pp. 1–6. [Online]. Available: http://dl.acm.org/citation.cfm?doid=3233188.3233211
[25] M. Aldrigo, M. Dragoman, and D. Dragoman, "Smart antennas based on graphene," *J. Appl. Phys.*, vol. 116, no. 11, Sep. 2014, Art. no. 114302.
[26] S. Abadal, I. Llatser, A. Mestres, H. Lee, E. Alarcón, and A. Cabellos-Aparicio, "Time-domain analysis of graphene-based miniaturized antennas for ultra-short-range impulse radio communications," *IEEE Trans. Commun.*, vol. 63, no. 4, pp. 1470–1482, Apr. 2015.
[27] J. M. Jornet and I. F. Akyildiz, "Graphene-based plasmonic nano-transceiver for terahertz band communication," in *Proc. 8th Eur. Conf. Antennas Propag., (EuCAP)*, 2014, pp. 492–496.
[28] R. Y. Deng, F. Yang, S. Xu, and M. Li, "An FSS-backed 20/30-GHz dual-band circularly polarized reflectarray with suppressed mutual coupling and enhanced performance," *IEEE Trans. Antennas Propag.*, vol. 65, no. 2, pp. 926–931, Feb. 2017.
[29] M. Jablan, H. Buljan, and M. Solja ić, "Plasmonics in graphene at infrared frequencies," *Phys. Rev. B, Condens. Matter*, vol. 80, no. 24, Dec. 2009, Art. no. 245435.
[30] S. Blanch, J. Romeu, and I. Corbella, "Exact representation of antenna system diversity performance from input parameter description," *Electron. Lett.*, vol. 39, no. 9, pp. 705–707, 2003.
[31] J. C. Vardaxoglou, *Frequency Selective Surfaces: Analysis and Design*. Hoboken, NJ, USA: Wiley, 1997.
[32] W. Fuscaldo, P. Burghignoli, P. Baccarelli, and A. Galli, "Complex mode spectra of graphene-based planar structures for THz applications," *J. Infr. Millim. Terahertz Waves*, vol. 36, no. 8, pp. 720–733, Aug. 2015.
[33] L. Zakrajsek, E. Einarsson, N. Thawdar, M. Medley, and J. M. Jornet, "Lithographically defined plasmonic graphene antennas for terahertz-band communication," *IEEE Antennas Wireless Propag. Lett.*, vol. 15, pp. 1553–1556, 2016. [Online]. Available: http://ieeexplore.ieee.org/document/7400975/
[34] V. Iberi *et al.*, "Maskless lithography and *in situ* visualization of conductivity of graphene using helium ion microscopy," *Sci. Rep.*, vol. 5, Dec. 2015, Art. no. 11952.
[35] J. M. Jornet and A. Cabellos, "On the feeding mechanisms for graphene-based THz plasmonic nano-antennas," in *Proc. IEEE 15th Int. Conf. Nanotechnol. (IEEE-NANO)*, Jul. 2015, pp. 168–171. [Online]. Available: http://ieeexplore.ieee.org/document/7388948/
[36] W. Zouaghi, D. Voß, M. Gorath, N. Nicoloso, and H. G. Roskos, "How good would the conductivity of graphene have to be to make single-layer-graphene metamaterials for terahertz frequencies feasible?" *Carbon*, vol. 94, pp. 301–308, Nov. 2015.
[37] W. Fuscaldo, P. Burghignoli, P. Baccarelli, and A. Galli, "Graphene fabry–perot cavity leaky-wave antennas: Plasmonic versus nonplasmonic solutions," *IEEE Trans. Antennas Propag.*, vol. 65, no. 4, pp. 1651–1660, Apr. 2017.

BIN ZHANG was born in Shanxi, China. He received the B.S. degree in physics from Yuncheng University, China, in 2012. He is currently pursuing the Ph.D. degree in information and communication engineering from the Wuhan University of Technology, Wuhan, China. He was a Visiting Scholar with the Broadband Wireless Network Laboratory, School of Electrical and Computer Engineering, Georgia Institute of Technology, Atlanta, GA, USA, under the guidance of Prof. I. F. Akyildiz, from 2016 to 2017. His current research interests include millimeter-wave and terahertz communications, graphene-based plasmonic devices, and electromagnetic wave propagation.

JOSEP M. JORNET (S'08–M'13) received the B.S. degree in telecommunication engineering and the M.Sc. degree in information and communication technologies from the Universitat Politecnica de Catalunya, Barcelona, Spain, in 2008, and the Ph.D. degree in electrical and computer engineering from the Georgia Institute of Technology (Georgia Tech), Atlanta, GA,USA, in 2013. From 2007 to 2008, he was a Visiting Researcher with the Massachusetts Institute of Technology (MIT), Cambridge, under the MIT Sea Grant Program. He is currently an Associate Professor with the Department of Electrical Engineering, University at Buffalo (UB), The State University of New York. His current research interests include terahertz-band communication networks, wireless nano-bio-sensing networks, and the Internet of Nano-Things. He was a recipient of the Oscar P. Cleaver Award for outstanding graduate students with the School of Electrical and Computer Engineering, Georgia Tech, in 2009, and the Broadband Wireless Networking Lab Researcher of the Year Award, in 2010. He also received the IEEE Communications Society Young Professional Best Innovation Award, the ACM NanoCom Outstanding Milestone Award, and the UB SEAS Early Career Researcher of the Year Award, in 2017, and the UB Exceptional Scholar Award-Young Investigator Award and the UB SEAS Early Career Teacher Award, in 2018.

IAN F. AKYILDIZ (M'86–SM'89–F'96) was an Adjunct Professor with the University of Pretoria, South Africa, from 2007 to 2012. He established the NanoNetworkingCenter and was an Adjunct Professor with the Politecnica Universitat de Catalunya, Barcelona, Spain, from 2007 to 2017. From 2012 to 2016, he was a FiDiPro (Finland Distinguished Professor) supported by the Academy of Finland with the Tampere University of Technology, Finland. Since 2011, he has been a Consulting Chair Professor with King Abdulaziz University in Jeddah, Saudi Arabia. He has been an Adjunct Professor with the University of Cyprus, since 2017. He has also been the Megagrant Leader with the Russian Academy of Sciences, Moscow, Russia, since 2018. He is currently the Ken Byers Chair Professor in telecommunications with the School of Electrical and Computer Engineering, Georgia Institute of Technology, Atlanta, the Director of the Broadband Wireless Networking Laboratory, and the Chair of the Telecommunication Group, Georgia Tech. His current research interests include nano-scale and molecular communication, terahertz communication, 5G and beyond wireless systems, and wireless communication in challenged environments, such as underwater and underground. He is an ACM Fellow, in 1997. He received numerous awards from the IEEE, ACM, and other organizations. He received the Humboldt Award to Conduct Research with the University of Erlangen-Nurnberg, from 2014 to 2016. He is the Editor-in-Chief of the *Computer Networks Journal* (Elsevier) and founding Editor-in-Chief of the *Ad Hoc Networks Journal* (Elsevier). He is also the founding and Emeritus Editor-in-Chief of the *Physical Communication Journal* (Elsevier), and the *NanoComnet Journal* (Elsevier).

ZHI P. WU received the B.S., M.S., and Ph.D. degrees in computer engineering from the University of Erlangen-Nuremberg, Germany, in 1978, 1981, and 1984, respectively. He is currently the Ken Byers Chair Professor in telecommunication and the Chair of the Telecommunications Group, School of Electrical and Computer Engineering, Georgia Institute of Technology, and the Director of the Broadband Wireless Networking Laboratory. He has been a Professor associated with the School of Information Engineering and the Hubei Engineering Research Center of RF-Microwave Technology and Application, Wuhan University of Technology, Wuhan, China. His current research interests include antennas, RF and microwave electronics, WSNs, and the Internet of Things.